Exact Solution of Non-Hermitian Systems with Generalized Boundary Conditions: Size-Dependent Boundary Effect and Fragility of the Skin Effect

Cui-Xian Guo,[1] Chun-Hui Liu,[1,2] Xiao-Ming Zhao,[1] Yanxia Liu,[1] and Shu Chen[1,2,3,*]
[1]*Beijing National Laboratory for Condensed Matter Physics, Institute of Physics, Chinese Academy of Sciences, Beijing 100190, China*
[2]*School of Physical Sciences, University of Chinese Academy of Sciences, Beijing 100049, China*
[3]*Yangtze River Delta Physics Research Center, Liyang, Jiangsu 213300, China*

(Received 9 February 2021; revised 8 June 2021; accepted 16 August 2021; published 9 September 2021)

Systems with non-Hermitian skin effects are very sensitive to the imposed boundary conditions and lattice size, and thus an important question is whether non-Hermitian skin effects can survive when deviating from the open boundary condition. To unveil the origin of boundary sensitivity, we present exact solutions for one-dimensional non-Hermitian models with generalized boundary conditions and study rigorously the interplay effect of lattice size and boundary terms. Besides the open boundary condition, we identify the existence of non-Hermitian skin effect when one of the boundary hopping terms vanishes. Apart from this critical line on the boundary parameter space, we find that the skin effect is fragile under any tiny boundary perturbation in the thermodynamic limit, although it can survive in a finite size system. Moreover, we demonstrate that the non-Hermitian Su-Schreieffer-Heeger model exhibits a new phase diagram in the boundary critical line, which is different from either open or periodical boundary case.

DOI: 10.1103/PhysRevLett.127.116801

Introduction.—It is well known that the spectrum of a periodic crystal can be characterized by the Bloch wave vector and the periodic boundary condition (PBC) is usually taken for the convenience of calculating the band structure [1]. If the system size is large enough, the bulk spectrum is stable against boundary perturbations even though the translation invariance of the system is broken [2–4]. This constitutes the foundation for understanding why the bulk energy levels of a large system with an open boundary condition (OBC) can be reproduced from the Bloch band calculation. However, such a paradigm is challenged in some non-Hermitian systems [5–9], for which the wave functions in large systems with OBC accumulate on the boundary accompanying with a remarkably different eigenvalue spectrum from the periodic system [10–16]. This phenomenon is coined as the non-Hermitian skin effect (NHSE) [9] and recently attracted intensive studies [17–33].

The NHSE suggests that the change of the boundary condition may induce dramatic change of bulk properties of non-Hermitian systems [9–16,34–40]. Size-dependent NHSEs are also observed in some coupled non-Hermitian chains [41,42] and nonreciprocal chains with impurity [43,44]. These studies indicate that both boundaries and lattice size play an important role in these boundary sensitive effects. Although the spectral flow from PBC to OBC is studied by introducing an imaginary flux [13,45], it is still elusive to get a quantitative understanding of the sharp change of spectrum and wave functions of skin modes under tiny boundary perturbations. A more challenging task is to quantitatively count the interplay effect of system size and boundary perturbations and unveil the intrinsic reason behind the boundary sensitive effects. As numerical methods for boundary sensitive problems are time consuming and sometimes unreliable due to the existence of numerical errors and calculation precision [46,47], exact solutions are highly desirable for analytically exploring the size-dependent boundary effect.

In this Letter, we present exact solutions of non-Hermitian models with nonreciprocal hopping under generalized boundary conditions (GBCs), which enable us to rigorously explore the interplay effect of lattice size and boundary perturbations. Our analytical results show explicitly how the lattice size and boundary terms affect the solutions of eigenequations. Particularly, we find the existence of NHSE in a critical line on the boundary parameter space, including the OBC as a special case. Apart from the critical line, the NHSE is unstable against any tiny boundary perturbations in the thermodynamic limit and thus is fragile, although it may survive in a finite size system. Moreover, we find that the two-band system can exhibit a new phase diagram in the critical line, which is different from either PBC or OBC case, but is a combination of the two cases. Our work demonstrates novel phenomena induced by the boundary terms from the perspective of an exact solution and provides a firm ground for understanding boundary sensitivity phenomena in non-Hermitian systems.

Hatano-Nelson model with generalized boundary conditions.—We start with the Hatano-Nelson (HN) model [48,49] with GBC described by

$$\hat{H} = \sum_{n=1}^{N-1} [t_L \hat{c}_n^\dagger \hat{c}_{n+1} + t_R \hat{c}_{n+1}^\dagger \hat{c}_n] + \delta_R \hat{c}_1^\dagger \hat{c}_N + \delta_L \hat{c}_N^\dagger \hat{c}_1, \quad (1)$$

where N is the number of lattice sites, $\delta_L, \delta_R \in \mathbb{R}$ determines the GBC, and $t_L, t_R \in \mathbb{R}$ are imbalanced hopping amplitudes which can be parametrized as $t_L = te^{-g}$ and $t_R = te^{g}$ with real t and g.

The eigenvalue equation $\hat{H}|\Psi\rangle = E|\Psi\rangle$ with $|\Psi\rangle = \sum_n \psi_n |n\rangle$ and $|n\rangle = \hat{c}_n^\dagger |0\rangle$ $(n = 1, \ldots, N)$consists of a series of equations, including bulk equations

$$t_R \psi_s - E\psi_{s+1} + t_L \psi_{s+2} = 0 \quad (2)$$

with $s = 1, \ldots, N-2$, and the boundary equations given by $-E\psi_1 + t_L\psi_2 + \delta_R\psi_N = 0$ and $\delta_L\psi_1 + t_R\psi_{N-1} - E\psi_N = 0$, which are equivalent to

$$t_R\psi_0 = \delta_R\psi_N, \qquad \delta_L\psi_1 = t_L\psi_{N+1}. \quad (3)$$

Because of spatial translational property from bulk equations, we set the ansatz of wave function Ψ_i which satisfies the bulk equations Eq. (2) as follows:

$$\Psi_i = (z_i, z_i^2, z_i^3, \ldots, z_i^{N-1}, z_i^N)^T. \quad (4)$$

By inserting Eq. (4) into Eq. (2), we obtain the expression of eigenvalue in terms of z_i:

$$E = \frac{t_R}{z_i} + t_L z_i. \quad (5)$$

For a given E, there are two solutions z_i (z_1, z_2), and thus they should fulfill the constraint condition as follows:

$$z_1 z_2 = \frac{t_R}{t_L}. \quad (6)$$

The superposition of these two linearly independent solutions is also the solution of Eq. (2), i.e., $\Psi = c_1\Psi_1 + c_2\Psi_2 = (\psi_1, \psi_2, \ldots, \psi_N)^T$, where $\psi_n = \sum_{i=1}^2 (c_i z_i^n) = c_1 z_1^n + c_2 z_2^n$ with $n = 1, 2, \ldots, N$.

To solve the eigenequation, the general ansatz of wave function should satisfy the boundary conditions. By inserting the expression of Ψ into Eq. (3), the boundary equations transforms into $H_B(c_1, c_2)^T = 0$ with

$$H_B = \begin{pmatrix} t_R - \delta_R z_1^N & t_R - \delta_R z_2^N \\ z_1(\delta_L - t_L z_1^N) & z_2(\delta_L - t_L z_2^N) \end{pmatrix}.$$

The condition for the existence of nontrivial solutions for (c_1, c_2), is determined by $\det[H_B] = 0$, which gives rise to the general solution as follows:

$$(z_1^{N+1} - z_2^{N+1}) - \frac{\delta_R\delta_L}{t_L^2}(z_1^{N-1} - z_2^{N-1}) - \left[\frac{\delta_L}{t_L} + \frac{\delta_R}{t_R}\left(\frac{t_R}{t_L}\right)^N\right](z_1 - z_2) = 0. \quad (7)$$

Equations (7) and (6) together determine the solution of z_1 and z_2 exactly. The solutions of z_1 and z_2 give the finite-size generalized Brillouin zone [9,14,15,50], which may be different for different lattice size. According to the constraint condition of Eq. (6), we can always set the solution as

$$z_1 = re^{i\theta}, \qquad z_2 = re^{-i\theta}, \quad (8)$$

with $r = \sqrt{(t_R/t_L)} = e^g$, then Eq. (7) becomes

$$\sin[(N+1)\theta] - \eta_1 \sin[(N-1)\theta] - \eta_2 \sin[\theta] = 0, \quad (9)$$

where $\eta_1 = (\delta_R\delta_L/t_R t_L)$ and $\eta_2 = (\delta_L/t_L)r^{-N} + (\delta_R/t_R)r^N = (\delta_L/t_L)e^{-gN} + (\delta_R/t_R)e^{gN}$. The corresponding eigenvalue is given by

$$E = 2\sqrt{t_R t_L}\cos\theta. \quad (10)$$

The solutions θ of Eq. (9) may take real or complex depending on the values of η_1 and η_2. In the presence of both nonzero boundary terms, i.e., with fixed $\delta_{L,R} \neq 0$, η_2 always increases exponentially with N [51], and thus the solutions are very sensitive to even a tiny boundary perturbation since the perturbation is amplified exponentially by a factor e^{gN} $(g > 0)$ or e^{-gN} $(g < 0)$, which is the origin of size-dependent boundary sensitivity. Such a size-enhancing boundary sensitivity has no correspondence in the Hermitian limit with $g = 0$.

The OBC corresponds to $\delta_R = \delta_L = 0$, for which $\eta_1 = \eta_2 = 0$ and Eq. (9) has N real solutions given by $\theta = [m\pi/(N+1)]$ $(m = 1, \ldots, N)$. The corresponding eigenvalues are real with eigenstates given by $\Psi = (r\sin[\theta], \ldots, r^N \sin[N\theta])^T$. For cases with either $\delta_R = 0$ $(\delta_L \neq 0)$ or $\delta_L = 0$ $(\delta_R \neq 0)$, we have $\eta_1 = 0$ and $\eta_2 = (\delta_L/t_L)r^{-N}$ or $\eta_2 = (\delta_R/t_R)r^N$. As long as $|\eta_2| < 1$, Eq. (9) has N real solutions, and the corresponding eigenvalues given by Eq. (10) are real. Particularly, in the thermodynamic limit we have $|\eta_2| \to 0$ for the case of $\delta_R = 0$ and $r > 1$ or $\delta_L = 0$ and $r < 1$, and the solutions $\theta = [m\pi/(N+1)]$ are identical to the OBC case. The analytical results indicate clearly that in these cases the system exhibits NHSE as all wave functions accumulate either on the left $(r < 1)$ or right $(r > 1)$ edge in the large size limit.

Consider the general case with nonzero δ_L and δ_R. In the region of $0 < (\delta_R/t_R), (\delta_L/t_L) < 1$, we have $0 < \eta_1 < 1$ and $\eta_2 > 0$. When $\eta_2 < 1 + \eta_1$, Eq. (9) has N real solutions. When $\eta_2 > N + 1 - \eta_1(N-1)$ which always holds

true in the large N limit, Eq. (9) has no real solutions but N complex solutions, and the corresponding eigenvalues are complex. In the thermodynamic limit, $|z_{1/2}| \to 1$ and $|z_{2/1}| \to (t_R/t_L)$ suggest that the spectrum approaches to the periodic spectrum [52].

To give a concrete example, we display the energy spectra and averaged inverse participation ratio (IPR) in Fig. 1 for the case of $t_R/t_L < 1$ in the region of $0 \le (\delta_R/t_R), (\delta_L/t_L) \le 1$. The averaged IPR is defined as $\overline{\mathrm{IPR}} = (1/N)\sum_{s=1}^{N} \mathrm{IPR}_s = (1/N)\sum_{s=1}^{N}[\sum_n |\langle n|\Psi^s\rangle|^4/(\langle\Psi^s|\Psi^s\rangle)^2]$, where Ψ^s is the sth right eigenstate Ψ of H. While $\overline{\mathrm{IPR}} \sim (1/N)$ approaches zero in large N limit for homogeneously distributed eigenstates, a finite $\overline{\mathrm{IPR}}$ gives signature of NHSE. As shown in Fig. 1(A) for $N = 10$, the eigenstates in the yellow region are similar to the OBC case, and the corresponding eigenvalues are real as displayed in Figs. 1(a)–1(d). When we increase the size N, the yellow region becomes narrow. The eigenvalues with the same parameters as in Fig. 1(d) become complex as displayed in Figs. 1(e) and 1(f) for $N = 20$ and 80, respectively. Particularly, for $N = 80$, the spectrum almost completely overlaps with the PBC spectrum, and the blue region almost spreads over the whole parameter space except a very narrow region near the axis of $\delta_L = 0$, consistent with our analytic prediction.

For the special case of $c_2 = 0$, eigenfunction is composed of only one solution, i.e., $|\Psi\rangle = c_1|\Psi_1\rangle$, and the boundary equation $H_B(c_1, 0)^T = 0$ requires that

$$t_R = \delta_R z_1^N, \qquad \delta_L = t_L z_1^N, \tag{11}$$

which can be satisfied simultaneously only if

$$\frac{t_R}{\delta_R} = \frac{\delta_L}{t_L} = \mu. \tag{12}$$

Here $\mu = 1$ corresponds to the PBC. Under the boundary condition (12), the solution of z_1 is determined by $z_1^N = \mu$, which gives rise to $z_1 = \sqrt[N]{\mu} e^{i(2m\pi/N)}$, $(m = 1, \ldots, N)$. It then follows that the spectrum is given by

$$E = \left(t_L \sqrt[N]{\mu} + \frac{t_R}{\sqrt[N]{\mu}}\right)\cos(\theta) + i\left(t_L \sqrt[N]{\mu} - \frac{t_R}{\sqrt[N]{\mu}}\right)\sin(\theta) \tag{13}$$

with $\theta = (2m\pi/N)$, and eigenstates as $\Psi = [\sqrt[N]{\mu} e^{i\theta}, \ldots, (\sqrt[N]{\mu} e^{i\theta})^N]^T$. For the general case ($\mu \neq 1$), while the system may exhibit NHSE for a finite N, the NHSE disappears in the large size limit as $|z_1|$ always approaches 1 when $N \to \infty$ for a fixed μ, as displayed in Fig. 2 (here $z = z_1$). Therefore, this case is similar to the PBC case in the thermodynamic limit. If we take $\mu = r^N$, we have $E = 2\sqrt{t_L t_R}\cos\theta$ with $\theta = (2m\pi/N)$. This special case is the so called modified PBC studied in Ref. [22]. When $\mu = r^{2N}$, the system has the same spectrum as under PBC and we call it pseudo-PBC, as the corresponding wave functions exhibit NHSE. We also present the spectra flow of the HN model in the Supplemental Material [52].

Non-Hermitian Su-Schrieffer-Heeger model.—We can also exactly solve the one-dimensional (1D) non-Hermitian Su-Schrieffer-Heeger (SSH) model with GBC, described by

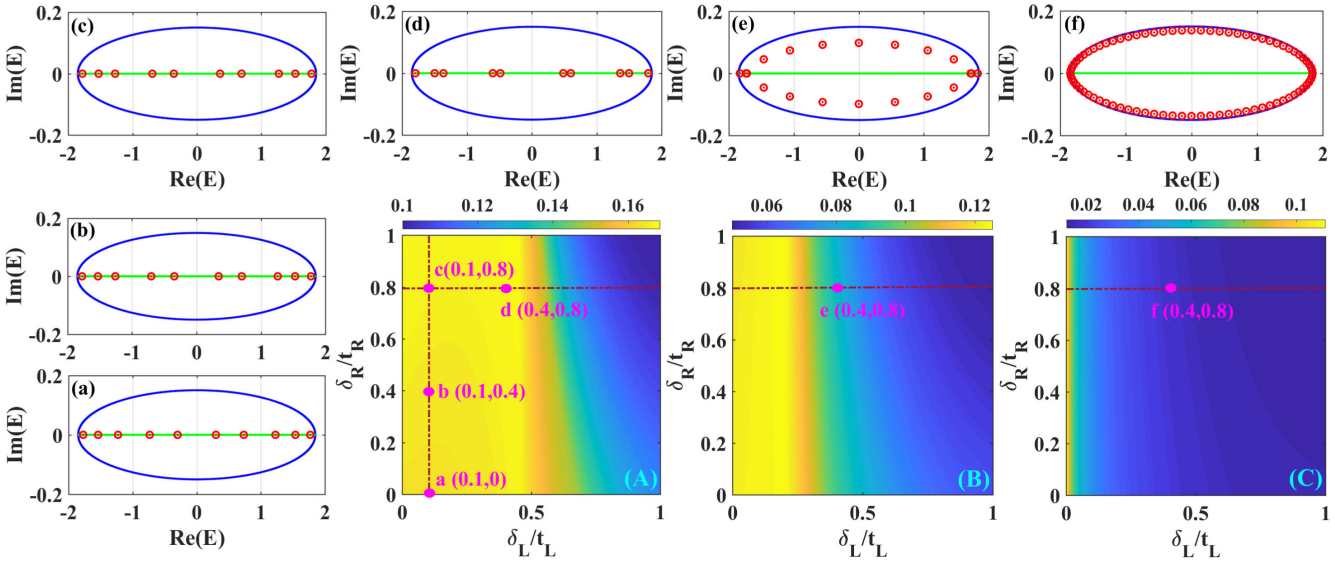

FIG. 1. (A)–(C) $\overline{\mathrm{IPR}}$ on the parameter space of δ_L/t_L and δ_R/t_R for HN model with $N = 10, 20, 80$, respectively. (a)–(f) Spectrum (red circles and dots) corresponding dots a–f in (A)–(C), respectively. The analytical results (red circles) are in exact agreement with the numerical results (red dots). The green and blue lines represent the spectrum corresponding to OBC and PBC case in the thermodynamic limit, respectively. Common parameters: $t_L = 1$, $t_R = 0.85$.

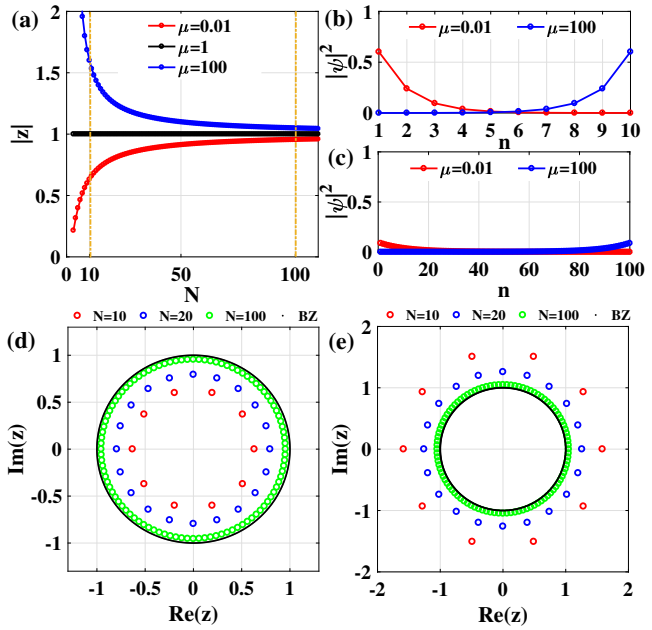

FIG. 2. (a) $|z|$ as a function of lattice size N for HN model with $\mu = 0.01,\ 1,\ 100$. (b),(c) The profile of all eigenstates with $N = 10$ and $N = 100$ independent of t_R, t_L, respectively. (d),(e) The finite-size generalized Brillouin zones z with $\mu = 0.01$ and $\mu = 100$ for different size $N = 10,\ 20,\ 100$ independent of t_R, t_L, respectively. The curve formed by black dots represents Brillouin zone for PBC case.

$$\hat{H} = \sum_n [t_{1L}\hat{c}^\dagger_{nA}\hat{c}_{nB} + t_{1R}\hat{c}^\dagger_{nB}\hat{c}_{nA} + t_{2R}\hat{c}^\dagger_{(n+1)A}\hat{c}_{nB} + t_{2L}\hat{c}^\dagger_{nB}\hat{c}_{(n+1)A}] + \delta_R\hat{c}^\dagger_{1A}\hat{c}_{MB} + \delta_L\hat{c}^\dagger_{MB}\hat{c}_{1A}, \tag{14}$$

where $t_{1L/1R}$ and $t_{2L/2R}$ are imbalanced hopping terms between intracell and intercell sites, and the summation of n is over M cells. The phase boundaries under PBC are determined by the gap closing condition [9,53–55]: $|t_{1R}/t_{2L}| = 1$ or $|t_{1L}/t_{2R}| = 1$, as shown in Fig. 3(a). All parameters $t_{1L/1R}$ and $t_{2L/2R}$ are taken to be positive.

In the same framework we can obtain the analytical solution of model (14) [52]. From the expression of E in terms of z_i, it follows that z_1 and z_2 fulfill the constraint condition as follows:

$$z_1 z_2 = \frac{t_{1R}t_{2R}}{t_{1L}t_{2L}}. \tag{15}$$

Similarly, the boundary equation leads to

$$(z_1^{M+1} - z_2^{M+1}) + \chi_1(z_1^M - z_2^M) - \chi_2(z_1^{M-1} - z_2^{M-1}) - \chi_3(z_1 - z_2) = 0, \tag{16}$$

with $\chi_1 = [(t_{2R}t_{2L} - \delta_R\delta_L)/t_{1L}t_{2L}]$, $\chi_2 = (t_{1R}\delta_R\delta_L/t_{1L}t_{2L}^2)$, and $\chi_3 = (\delta_L/t_{2L}) + (\delta_R/t_{2R})(t_{1R}t_{2R}/t_{1L}t_{2L})^M$. According to Eq. (15), we can always set the solution as the form of Eq. (8) with $r = \sqrt{(t_{1R}t_{2R}/t_{1L}t_{2L})}$. Then Eq. (16) becomes

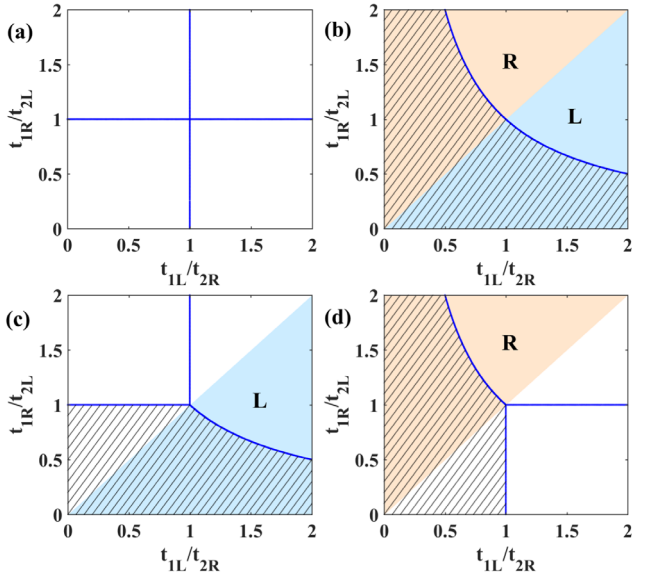

FIG. 3. Phase diagram for non-Hermitian SSH model (a) PBC case, (b) OBC case, (c) case of $\delta_L = 0$, $\delta_R \neq 0$, (d) case of $\delta_R = 0$, $\delta_L \neq 0$. The phase boundaries are denoted by blue lines, and bound states exist in the shadow region. The bulk states in the blue region and orange region are located at the left and right edge, respectively. There is no NHSE in the white region.

$$\sin[(M+1)\theta] + \eta_1 \sin[M\theta] - \eta_2 \sin[(M-1)\theta] = \eta_3 \sin[\theta], \tag{17}$$

where $\eta_1 = [(t_{2R}t_{2L} - \delta_R\delta_L)/\sqrt{t_{1R}t_{2R}t_{1L}t_{2L}}]$, $\eta_2 = (\delta_R\delta_L/t_{2R}t_{2L})$, and $\eta_3 = (\delta_L/t_{2L})r^{-M} + (\delta_R/t_{2R})r^M$.

For the OBC case, we have $\eta_2 = \eta_3 = 0$ and $\eta_1 = \alpha$ with $\alpha = \sqrt{(t_{2R}t_{2L}/t_{1R}t_{1L})}$. While Eq. (17) has M real solutions corresponding to bulk states when $\alpha < \alpha_c$, it has $M-1$ real solutions corresponding to bulk states and one complex solution ($\theta = \pi + i\varphi$) corresponding to edge states when $\alpha > \alpha_c$. In the thermodynamic limit, $\alpha_c = 1 + (1/M) \to 1$, and thus the boundary of topological phase transition is given by $\alpha = 1$, i.e., $t_{2R}t_{2L} = t_{1R}t_{1L}$ as shown in Fig. 3(b).

For the case with $\delta_L = 0$ and $\delta_R \neq 0$, we have $\eta_1 = \alpha$, $\eta_2 = 0$ and $\eta_3 = (\delta_R/t_{2R})r^M$. In the thermodynamic limit, $\eta_3 \to 0$ for $r < 1$, and the solutions of θ are identical to the OBC case, whereas $\eta_3 \to \infty$ for a finite δ_R/t_{2R} when $r > 1$. It follows that Eq. (17) has no real solutions but M complex solutions, and $|z_1| \to 1$ and $|z_2| \to (t_{1R}t_{2R}/t_{1L}t_{2L})$ for bulk states as $M \to \infty$. In this case, the spectrum in the thermodynamic limit approaches to the periodical spectrum. Since the spectra in the regions of $r < 1$ and $r > 1$ take different forms, the phase diagram should display different behaviors in these regions as shown in Fig. 3(c). While the phase boundary in the region of $r < 1$ is similar to OBC case, it is similar to PBC case in the region of $r > 1$.

For the other case with $\delta_R = 0$ and $\delta_L \neq 0$, we have $\eta_3 = (\delta_L/t_{2L})r^{-M}$. In the large M limit, $\eta_3 \to 0$ for $r > 1$

and $\eta_3 \to \infty$ for $r < 1$. Similarly, we can get the phase diagram as shown in Fig. 3(d). The phase boundaries in Figs. 3(c) and 3(d) are determined by the gap closing conditions. In the shadow regions, there exist in-gap bound states. In contrast to the OBC case, only left or right skin states exist in Fig. 3(c) or Fig. 3(d).

In the presence of finite δ_L and δ_R, Eq. (17) does not support real solutions in the large M limit, and the spectrum approaches the spectrum of the PBC case. Similar to the HN model, in the thermodynamic limit the NHSE is unstable to the perturbation with both $\delta_L \neq 0$ and $\delta_R \neq 0$, while it may exist in the finite size system.

Conclusions.—We exactly solved the non-Hermitian HN model and SSH model with GBCs and predicted the existence of NHSE beyond the OBC when one of the boundary hopping terms is absent. Apart from this critical line on the boundary parameter space, the NHSE is unstable under tiny boundary perturbations and vanishes in the thermodynamic limit, whereas it may exist in a finite size system. Based on the analytical results, we uncovered the origin of size-dependent NHSE and gave quantitative description of the interplay effect of boundary hopping terms and lattice size. We also applied our analytical results to explore the phase diagram of non-Hermitian SSH model under different boundary conditions and identified a novel phase diagram in the critical boundary line. The fragility of NHSE under boundary perturbations can be also found in other 1D nonreciprocal systems and even higher-dimensional systems with NHSE [23,56]. Consider a n-dimensional nonreciprocal system which exhibits NHSE under OBC, if we add a boundary perturbation along one of directions and take PBC in the other $n-1$ directions, the higher-dimensional system can be mapped to a 1D nonreciprocal system with GBC by applying Fourier transformation. Then we can conclude the existence of fragility of NHSE by following similar calculations in 1D systems. We give examples of two-dimensional (2D) models in the Supplemental Material [52] and numerically confirm the fragility of NHSE in the large-size limit under tiny boundary perturbations along both x and y directions.

The work is supported by National Key Research and Development Program of China (2016YFA0300600), NSFC under Grant No. 11974413, and the Strategic Priority Research Program of Chinese Academy of Sciences under Grant No. XDB33000000.

*Corresponding author.
schen@iphy.ac.cn

[1] N. W. Ashcroft and N. D. Mermin, *Solid State Physics* (Holt, Rinehart and Winston, New York, 1976).
[2] A. Alase, E. Cobanera, G. Ortiz, and L. Viola, Generalization of Bloch's theorem for arbitrary boundary conditions: Theory, Phys. Rev. B **96**, 195133 (2017).
[3] A. Alase, E. Cobanera, G. Ortiz, and L. Viola, Exact Solution of Quadratic Fermionic Hamiltonians for Arbitrary Boundary Conditions, Phys. Rev. Lett. **117**, 076804 (2016).
[4] F. K. Kunst, G. van Miert, and E. J. Bergholtz, Extended Bloch theorem for topological lattice models with open boundaries, Phys. Rev. B **99**, 085427 (2019).
[5] T. E. Lee, Anomalous Edge State in a Non-Hermitian Lattice, Phys. Rev. Lett. **116**, 133903 (2016).
[6] Y. Xiong, Why does bulk boundary correspondence fail in some non-Hermitian topological models, J. Phys. Commun. **2**, 035043 (2018).
[7] V. M. Martinez Alvarez, J. E. Barrios Vargas, and L. E. F. Foa Torres, Non-Hermitian robust edge states in one dimension: Anomalous localization and eigenspace condensation at exceptional points, Phys. Rev. B **97**, 121401(R) (2018).
[8] D. Leykam, K. Y. Bliokh, C. Huang, Y. D. Chong, and F. Nori, Edge Modes, Degeneracies, and Topological Numbers in Non-Hermitian Systems, Phys. Rev. Lett. **118**, 040401 (2017).
[9] S. Yao and Z. Wang, Edge States and Topological Invariants of Non-Hermitian Systems, Phys. Rev. Lett. **121**, 086803 (2018).
[10] H. Shen, B. Zhen, and L. Fu, Topological Band Theory for Non-Hermitian Hamiltonians, Phys. Rev. Lett. **120**, 146402 (2018).
[11] F. K. Kunst, E. Edvardsson, J. C. Budich, and E. J. Bergholtz, Biorthogonal Bulk-Boundary Correspondence in Non-Hermitian Systems, Phys. Rev. Lett. **121**, 026808 (2018).
[12] S. Yao, F. Song, and Z. Wang, Non-Hermitian Chern Bands, Phys. Rev. Lett. **121**, 136802 (2018).
[13] C. H. Lee and R. Thomale, Anatomy of skin modes and topology in non-Hermitian systems, Phys. Rev. B **99**, 201103(R) (2019).
[14] K. Yokomizo and S. Murakami, Non-Bloch Band Theory of Non-Hermitian Systems, Phys. Rev. Lett. **123**, 066404 (2019).
[15] K. Zhang, Z. Yang, and C. Fang, Correspondence between Winding Numbers and Skin Modes in Non-Hermitian Systems, Phys. Rev. Lett. **125**, 126402 (2020).
[16] N. Okuma, K. Kawabata, K. Shiozaki, and M. Sato, Topological Origin of Non-Hermitian Skin Effects, Phys. Rev. Lett. **124**, 086801 (2020).
[17] H. Jiang, L. J. Lang, C. Yang., S. L. Zhu, and S. Chen, Interplay of non-Hermitian skin effects and Anderson localization in nonreciprocal quasiperiodic lattices, Phys. Rev. B **100**, 054301 (2019).
[18] L. Jin and Z. Song, Bulk-boundary correspondence in a non-Hermitian system in one dimension with chiral inversion symmetry, Phys. Rev. B **99**, 081103(R) (2019).
[19] D. S. Borgnia, A. J. Kruchkov, and R.-J. Slager, Non-Hermitian Boundary Modes, Phys. Rev. Lett. **124**, 056802 (2020).
[20] S. Longhi, Probing non-Hermitian skin effect and non-Bloch phase transitions, Phys. Rev. Research **1**, 023013 (2019).
[21] L. Herviou, J. H. Bardarson, and N. Regnault, Defining a bulk-edge correspondence for non-Hermitian Hamiltonians

via singular-value decomposition, Phys. Rev. A **99**, 052118 (2019).
[22] K.-I. Imura and Y. Takane, Generalized bulk-edge correspondence for non-Hermitian topological systems, Phys. Rev. B **100**, 165430 (2019).
[23] C. H. Lee, L. Li, and J. Gong, Hybrid Higher-Order Skin-Topological Modes in Non-Reciprocal Systems, Phys. Rev. Lett. **123**, 016805 (2019).
[24] T. S. Deng and W. Yi, Non-Bloch topological invariants in a non-Hermitian domain-wall system, Phys. Rev. B **100**, 035102 (2019).
[25] M. Ezawa, Non-Hermitian boundary and interface states in nonreciprocal higher-order topological metals and electrical circuits, Phys. Rev. B **99**, 121411(R) (2019).
[26] Y. X. Liu and S. Chen, Diagnosis of bulk phase diagram of nonreciprocal topological lattices by impurity modes, Phys. Rev. B **102**, 075404 (2020).
[27] X. R. Wang, C. X. Guo, and S. P. Kou, Defective edge states and anomalous bulk-boundary correspondence in non-Hermitian topological systems, Phys. Rev. B **101**, 121116 (R) (2020).
[28] Z. Yang, K. Zhang, C. Fang, and J. Hu, Non-Hermitian Bulk-Boundary Correspondence and Auxiliary Generalized Brillouin Zone Theory, Phys. Rev. Lett. **125**, 226402 (2020).
[29] Y. Yi and Z. Yang, Non-Hermitian Skin Modes Induced by On-Site Dissipations and Chiral Tunneling Effect, Phys. Rev. Lett. **125**, 186802 (2020).
[30] Z. Gong, Y. Ashida, K. Kawabata, K. Takasan, S. Higashikawa, and M. Ueda, Topological Phases of Non-Hermitian Systems, Phys. Rev. X **8**, 031079 (2018).
[31] K. Kawabata, K. Shiozaki, M. Ueda, and M. Sato, Symmetry and Topology in Non-Hermitian Physics, Phys. Rev. X **9**, 041015 (2019).
[32] H. Zhou and J. Y. Lee, Periodic table for topological bands with non-Hermitian symmetries, Phys. Rev. B **99**, 235112 (2019).
[33] C.-H. Liu and S. Chen, Topological classification of defects in non-Hermitian systems, Phys. Rev. B **100**, 144106 (2019).
[34] Z. Ozcakmakli Turker and C. Yuce, Open and closed boundaries in non-Hermitian topological systems, Phys. Rev. A **99**, 022127 (2019).
[35] Y. Ashida, Z. Gong, and M. Ueda, Non-Hermitian Physics, Adv. Phys. **69**, 249 (2020).
[36] F. K. Kunst and V. Dwivedi, Non-Hermitian systems and topology: A transfer-matrix perspective, Phys. Rev. B **99**, 245116 (2019).
[37] R. Chen, C.-Z. Chen, B. Zhou, and D.-H. Xu, Finite-size effects in non-Hermitian topological systems, Phys. Rev. B **99**, 155431 (2019).
[38] J. C. Budich and E. J. Bergholtz, Non-Hermitian Topological Sensors, Phys. Rev. Lett. **125**, 180403 (2020).
[39] K. Kawabata, N. Okuma, and M. Sato, Non-Bloch band theory of non-Hermitian Hamiltonians in the symplectic class, Phys. Rev. B **101**, 195147 (2020).
[40] R. Koch and J. C. Budich, Bulk-boundary correspondence in non-Hermitian systems: Stability analysis for generalized boundary conditions, Eur. Phys. J. D **74**, 70 (2020).
[41] L. Li, C. H. Lee, S. Mu, and J. Gong, Critical non-Hermitian skin effect, Nat. Commun. **11**, 5491 (2020).
[42] C.-H. Liu, K. Zhang, Z. Yang, and S. Chen, Helical damping and dynamical critical skin effect in open quantum systems, Phys. Rev. Research **2**, 043167 (2020).
[43] L. Li, C. H. Lee, and J. Gong, Impurity induced scale-free localization, Commun. Phys. **4**, 42 (2021).
[44] S. Longhi, Loschmidt echo and fidelity decay near an exceptional point, Ann. Phys. (Berlin) **531**, 1900054 (2019).
[45] C. H. Lee, L. Li, R. Thomale, and J. Gong, Unraveling non-Hermitian pumping: Emergent spectral singularities and anomalous responses, Phys. Rev. B **102**, 085151 (2020).
[46] M. J. Colbrook, B. Roman, and A. C. Hansen, How to Compute Spectra with Error Control, Phys. Rev. Lett. **122**, 250201 (2019).
[47] L. Reichel and L. N. Trefethen, Eigenvalues and pseudo-eigenvalues of Toeplitz matrices, Linear Algebra Appl. **162–164**, 153 (1992).
[48] N. Hatano and D. R. Nelson, Localization Transitions in Non-Hermitian Quantum Mechanics, Phys. Rev. Lett. **77**, 570 (1996).
[49] N. Hatano and D. R. Nelson, Vortex pinning and non-Hermitian quantum mechanics, Phys. Rev. B **56**, 8651 (1997).
[50] Finite-size generalized Brillouin zone is introduced to express precisely generalized Brillouin zone for a finite non-Hermitian system.
[51] Here we keep $\delta_{L,R}$ fixed, i.e., as the values are given, they do not change with the size N. So η_2 always increases exponentially with N.
[52] See Supplemental Material at http://link.aps.org/supplemental/10.1103/PhysRevLett.127.116801 for (i) discussion of the solution for HN model, (ii) spectral flow of HN model, (iii) some details of exact solution of the non-Hermitian SSH model with generalized boundary consition, and (iv) fragility of NHSE for 2D models with generalized boundary condition.
[53] C. Yin, H. Jiang, L. Li, R. Lü, and S. Chen, Geometrical meaning of winding number and its characterization of topological phases in one-dimensional chiral non-Hermitian systems, Phys. Rev. A **97**, 052115 (2018).
[54] S. Lieu, Topological phases in the non-Hermitian Su-Schrieffer-Heeger model, Phys. Rev. B **97**, 045106 (2018).
[55] H. Jiang, R. Lü, and S. Chen, Topological invariants, zero mode edge states and finite size effect for a generalized non-reciprocal Su-Schrieffer-Heeger model, Eur. Phys. J. B **93**, 125 (2020).
[56] T. Liu, Y.-R. Zhang, Q. Ai, Z. Gong, K. Kawabata, M. Ueda, and F. Nori, Second-Order Topological Phases in Non- Hermitian Systems, Phys. Rev. Lett. **122**, 076801 (2019).